An Experimental Study of Heat Transfer from a Heated Flat Plate to a Circular Impinging Jet

Author

Mohammad Zandsalimy

December 16, 2021

Abstract

An experiment is conducted on the heat transfer during the impingement of an air jet onto a heated flat plate. The air jet is located directly above the center point of the plate and is impinging on the plate at a right angle. The goal is to characterize the forced convection heat transfer with Nusselt number and heat transfer coefficients. Further, the effect of Reynolds number and the distance between the nozzle and the plate on the heat transfer rate are also investigated. Increasing the Reynolds number results in an increment in convection heat transfer. Further, increasing the value of H/d also increases heat transfer.

Contents

List of Figures

List of Tables

Nomenclature

ϵ	Plate emissivity
ρ	Air density
σ	Stefan-Boltzmann constant
A	plate area
d	Nozzle diameter
H	Nozzle distance from the surface
h	Heat transfer coefficient
k	Heat conduction coefficient
Q	Volumetric flow rate
q	Heat transfer
r	Radial distance
T	Temperature
x	Rotameter height
Nu	Nusselt number
Pr	Prandtl number
Re	Reynolds number

1 Introduction

A jet impinging a surface is an important phenomenon in the fields of fluid mechanics and heat transfer. This technique can be used to increase heat transfer between the fluid and the surface. We seek to understand the flow field and mechanisms of impinging jets with the goal of identifying preferred methods of predicting jet performance. Impinging jets provide an effective and flexible way to transfer energy or mass in industrial applications. A directed liquid or gaseous flow released against a surface can efficiently transfer large amounts of thermal energy or mass between the surface and the fluid. Heat transfer applications include cooling of stock material during material forming processes, heat treatment, cooling of electronic components, heating of optical surfaces for defogging, cooling of turbine components, cooling of critical machinery structures, and many other industrial processes. Typical mass transfer applications include drying and removal of small surface particulates. Abrasion and heat transfer by impingement is also studied as side effects of vertical/short take-off and landing jet devices, for example in the case of direct lift propulsion systems in vertical/short take-off and landing aircraft. An experiment is a setup here for studying the forced convection heat transfer above a heated flat plate where a single turbulent air jet impinging on the surface.

1.1 Objectives

The main objectives of this experiment are:

- To familiarize with some basic equipment used in fluid flow and heat transfer experiments
- Practice the uncertainty analysis
- Develop skills in data reduction and technical report writing
- Compare results with available correlations in the literature

1.2 Experimental Setup

A schematic illustration of the experimental setup is presented in figure 1. The experimental setup consists of a compressed air supply system, a long pipe, and a heated impinging surface (test plate). The test plate (stainless steel 303 with dimensions of $8.8 \times 8.5 \times 0.25$ in^3) is designed to provide a known heat flux and allow measurement of the temperature at various locations The test plate and the jet nozzle is shown in figure 2. The impingement jet is aligned so that it hits the center of the plate where thermocouple #1 is installed. Thirty one thermocouples are embedded in the test plate which are shown in figure 3 (dimensions are in inches). It should be mentioned that thermocouple #24 is not present in our results. Thermocouples are connected to a data acquisition and control system (Agilent 34970A) hooked to a desktop computer. The data acquisition and control system is shown in figure 4. Six strip heaters are bounded to the back side of the test plate. The ensemble of the plate

and heaters is installed in a box (made of wood) filled with thermal insulation for minimizing heat losses as in figure 1.

A DC power supply is used ensuring continuously adjustable and stable power inputs to these heaters. At steady state condition, the local heat transfer coefficient is obtained knowing the local heat flux and the local temperature at the plate surface. The local surface heat flux is obtained knowing the total power supply to the heaters and accounting for radiation heat losses from the plate surface and heat losses through the insulation system. An infrared thermometer is used to estimate the surface emissivity. A heat flux meter installed within the plate insulation system is used for estimating the rate of heat losses from the strip heaters. Compressed air essentially at room temperature is used as the working fluid, and its flow rate is measured using rotameters which are shown in figure 5. The air temperature is measured using an inline thermocouple. In this setup, air flows through a long glass tube (12 inches long with an inner diameter of 0.156 in) to obtain a fully developed turbulent circular jet. A schematic view of the nozzle assembly is shown in figure 6. The local Nusselt numbers will be obtained for various Reynolds numbers ranging from 12000 to about 20000. For a given Reynolds number, the effects of the jet-exit to impingement-plate separations will be studied. The obtained results will be compared with the experimental correlations available in the literature.

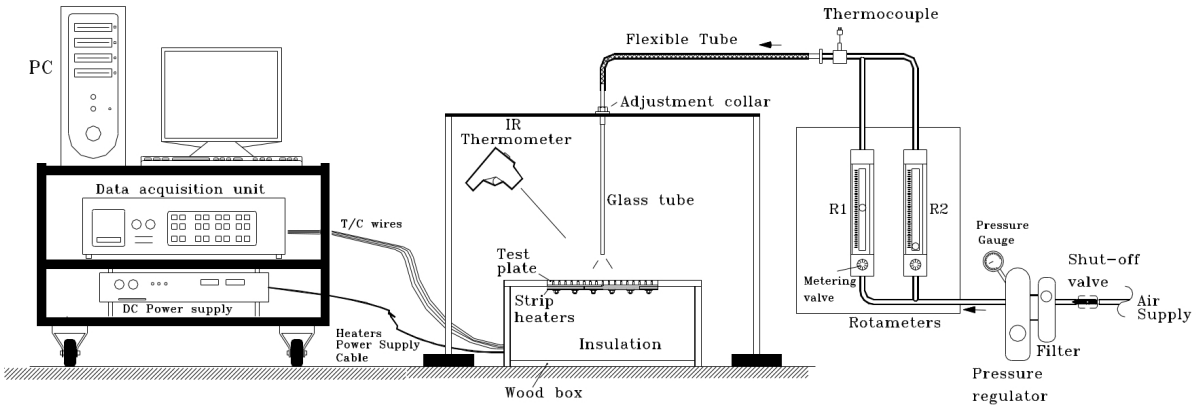

Figure 1: Schematic view of the test setup.

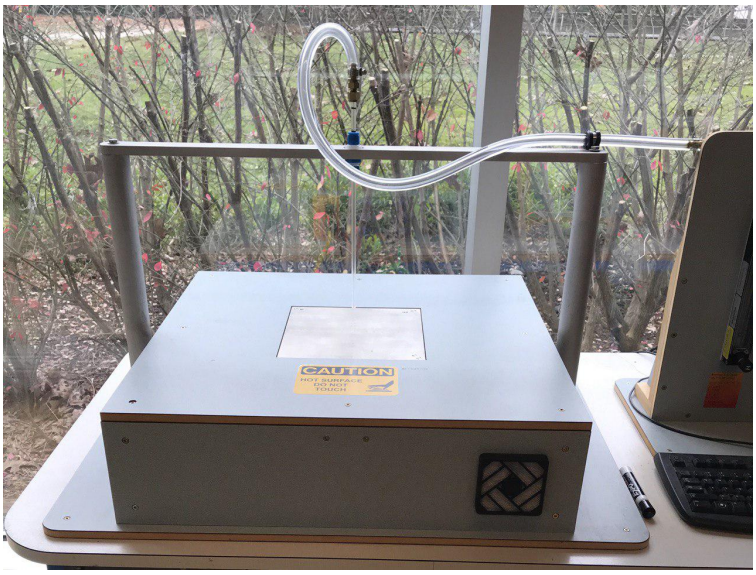

Figure 2: Test plate and the jet nozzle.

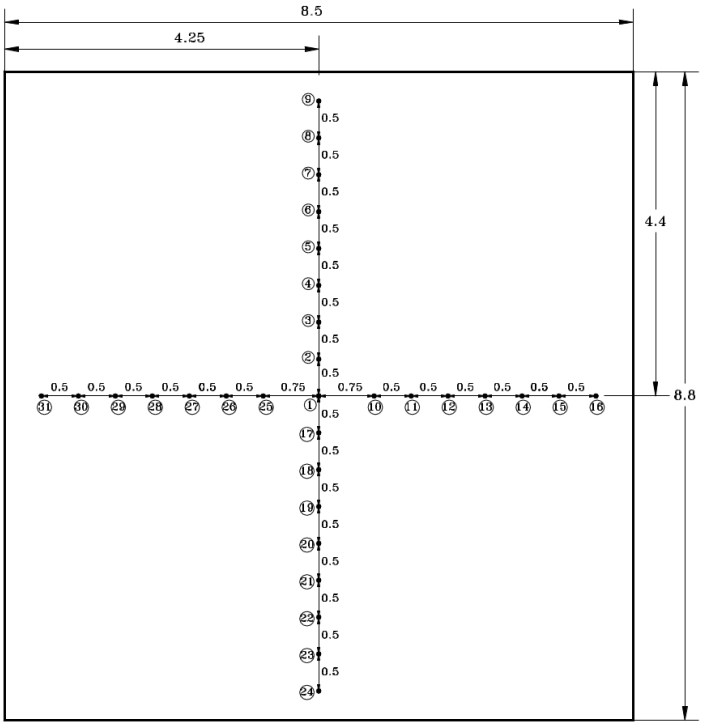

Figure 3: Thermocouple positions on the test plate.

Figure 4: Data acquisition and control module.

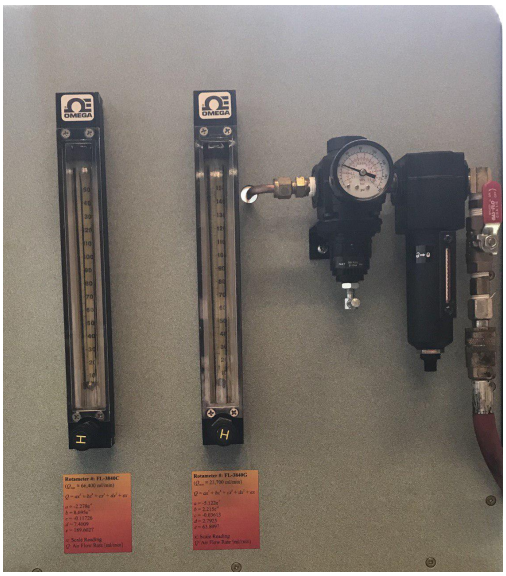

Figure 5: Rotameters in use.

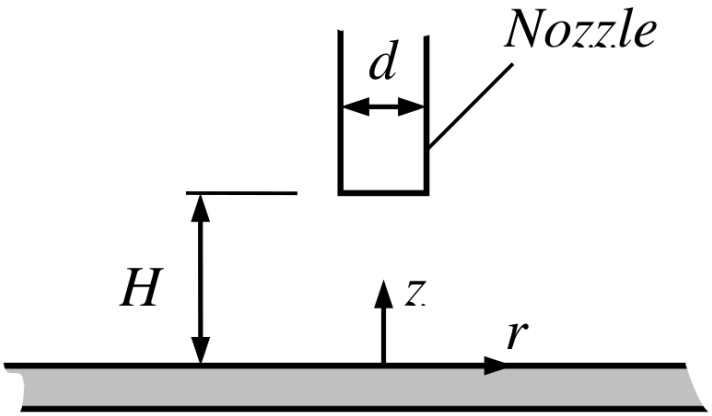

Figure 6: Nozzle assembly.

2 Theory

A schematic view of the geometry of the problem is presented in figure 7. In a typical impinging jet configuration, one can identify three distinct flow areas: the free jet, the impact zone and the wall jet [1]. The free jet is the area where the jet is not affected by the wall. Its flow is very similar to that of a free jet. In this area, a potential cone is formed, defined as the distance between the injection point and the point where the velocity gradient in the direction of the jet is not zero. The impact area starts when the jet is influenced by the presence of the wall. Lateral velocity increases rapidly when the jet approaches the wall. The flow field contains the stagnation point where the longitudinal velocity becomes zero. The last zone is that of the wall jet where the flow runs parallel to the wall and a boundary layer develops.

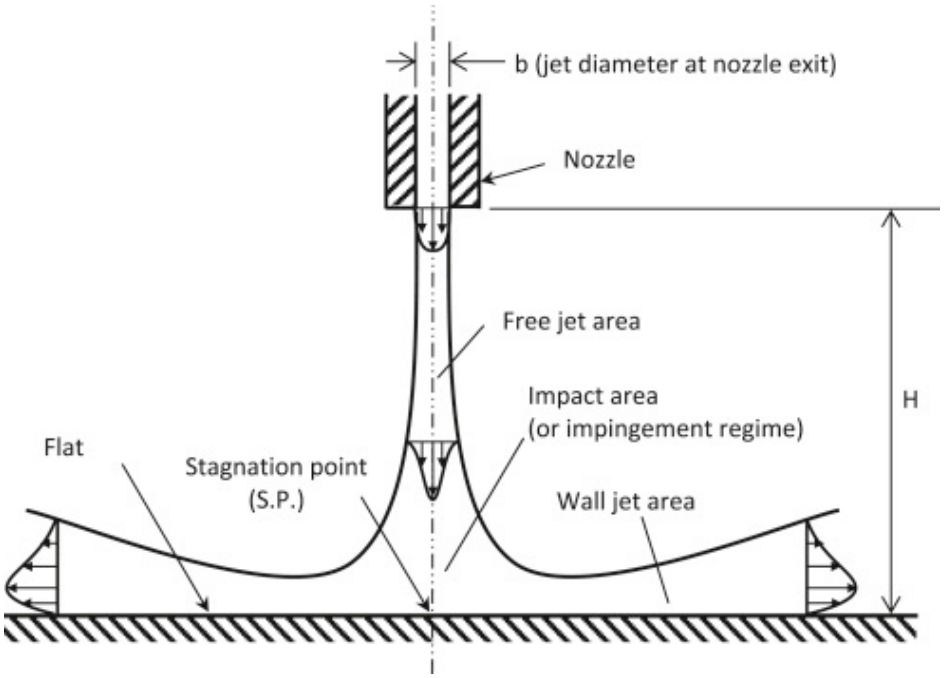

Figure 7: A schematic view of an impinging jet on a flat plate.

Compared to other heat or mass transfer arrangements that do not employ phase change, the jet impingement device offers efficient use of the fluid, and high transfer rates. For example, compared with conventional convection cooling by confined flow parallel to (under) the cooled surface, jet impingement produces heat transfer coefficients that are up to three times higher at a given maximum flow speed, because the impingement boundary layers are much thinner, and often the spent flow after the impingement serves to turbulate the surrounding fluid. Given a required heat transfer coefficient, the flow required from an impinging jet device may be two orders of magnitude smaller than that required for a cooling approach using a free wall-parallel flow. For more uniform coverage over larger surfaces multiple jets may be used. The impingement cooling approach also offers a compact hardware arrangement.

3 Test Procedure

The distance between the nozzle and the plate was set to $\frac{H}{d} = 10$ as shown in figure 8. Then, the input power is set to 100W by adjusting the DC power supply voltage. We have to get a Reynolds number of 20000 (based on the nozzle inner diameter by changing the flow rate with the rotameter. The volumetric flow rate of the rotameter is presented as equation 1. The coefficients in this equation are given in table 1. For a Reynolds number of 20000 we need the rotameter to be at $x = 129$ by solving for Re in equation 2. And for a Reynolds number of 12000 we will get $x = 86$. The inner diameter of the nozzle is 0.00382 m. After this step, we should wait for the system to reach steady state conditions to record all the temperature data, heat flux meter data, total power input, airflow rate and temperature,

and ambient air temperature. Then, we use the IR thermometer to estimate the emissivity of the plate. This value is found to be $\epsilon = 0.23$. After all the measurements, the airflow and input power are shut off. The same experiment should be conducted for a combination of two Reynolds numbers of 12000 and 20000, and $\frac{H}{d}$ =2.5 and 10.

Figure 8: Close view of the jet nozzle and plate.

$$Q = ax^5 + bx^4 + cx^3 + dx^2 + ex \tag{1}$$

$$Re = \frac{\rho V d}{\mu} = \frac{4\rho Q}{\pi D \mu} \tag{2}$$

Table 1: Correlation coefficients for the rotameter.

Coefficient	Value
a	-2.278×10^{-6}
b	8.695×10^{-4}
c	-0.11726
d	7.4009
e	189.6027

4 Results

In this section, the results of the experiments are presented. Test cases are named as presented in table 2 (test matrix). The average temperature is calculated for each case with the last 50 readings. The uncertainty in temperature reading is calculated using the

root mean squared method as in equation 3. The radiation heat transfer can be calculated using equation 4. In this equation, σ is the Stefan-Boltzmann constant and is equal to $5.6703 \times 10^{-8} \frac{\mathrm{W}}{m^2 K^4}$.

Table 2: Different test cases.

Test	Reynolds	$\frac{H}{d}$
T_1	12000	2.5
T_2	12000	10
T_3	20000	2.5
T_4	20000	10

$$u_T = \sqrt{\frac{\sum (T_i - \overline{T})^2}{N}} \tag{3}$$

$$q_{\text{radiation}} = \epsilon \sigma A (\overline{T}^4 - T_\infty^4) \tag{4}$$

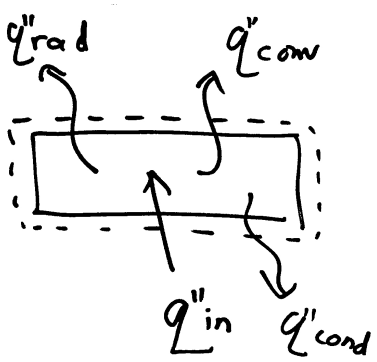

Figure 9: Heat transfer to the flat plate.

The schematic of different heat transfers to the plate are shown in figure 9. The heat transfer to the flat plate can be reported as in equation 5.

$$q_{\text{convection}} = q_{\text{input}} - q_{\text{radiation}} - q_{\text{conduction}} \tag{5}$$

This equation can be rewritten in the following form.

$$h(\overline{T} - T_\infty) = \frac{q_{\text{input}}}{A} - \epsilon \sigma (\overline{T}^4 - T_\infty^4) - q_{\text{conduction}} \tag{6}$$

From which we can find the local heat transfer coefficient. And then, the local Nusselt number can be found using the following equation.

$$\mathrm{Nu} = \frac{hd}{k} \tag{7}$$

In which k in the thermal conductivity of air which is equal to 0.0257 $\frac{W}{mK}$. The difference between air temperature and flat plate is not very high. As a result, we can ignore the changes in air properties and the thermal conductivity for air is assumed to be constant. The uncertainties in Nu number are calculated using the method presented in section "Uncertainty Analysis".

We assume that there are no uncertainties for d and k. As a result the uncertainty of Nu is equal to uncertainty of h.

$$u_{\mathrm{Nu}} = u_h \tag{8}$$

As a result, we just need to calculate the uncertainty in h according to the following equation.

$$u_h = \left[(\frac{\partial h}{\partial q_{\mathrm{input}}} u_{q_{\mathrm{input}}})^2 + (\frac{\partial h}{\partial q_{\mathrm{conduction}}} u_{q_{\mathrm{conduction}}})^2 + (\frac{\partial h}{\partial \overline{T}} u_{\overline{T}})^2 + (\frac{\partial h}{\partial T_\infty} u_{T_\infty})^2 \right]^{\frac{1}{2}} \tag{9}$$

These uncertainties are reported as error bars in our plots. The percentage probability (confidence level) is 99%.

4.1 Local Nusselt Number

In this section the local Nusselt number is plotted vs. r/d, where r is the radial distance from the center, for each case. Figures 10, 11, 12, and 13 show the local Nusselt number as a function of r/d for cases T_1, T_2, T_3, and T_4 (presented in table 2), respectively. These figures divide the measurements into five parts. First one is always for the stagnation channel, and other four lines show each of the four sides of the measurement array. Keep in mind that channel 24 has not given any data. As seen in these figures, the local Nusselt number decreases with r/d for all cases. comparing cases T_1 with T_3, and T_2 with T_4 we can see that increasing Reynolds number results in an increment in local Nusselt. Further, increasing the H/d ratio at a constant Reynolds also increases the local Nusselt distribution in the radial position. Furthermore, by moving far enough from the stagnation point, the changes in local Nusselt are getting smaller by a fair bit. As a result, we have larger changes in the local Nusselt to about $r/d = 15$, while for $r/d > 15$ those changes are very small for all test cases. The stagnation Nusselt is always the largest among the tests. Figure 14 shows the value of the Nusselt for channels 1 through 9 at each r/d for test cases T_1, T_2, T_3, and T_4. As seen in this figure our conclusion on changes of local Nusselt with Reynolds number and H/d was in fact correct. As a result we can conclude that at higher Reynolds numbers we can get more cooling effect while increasing H/d, decreases the cooling effect.

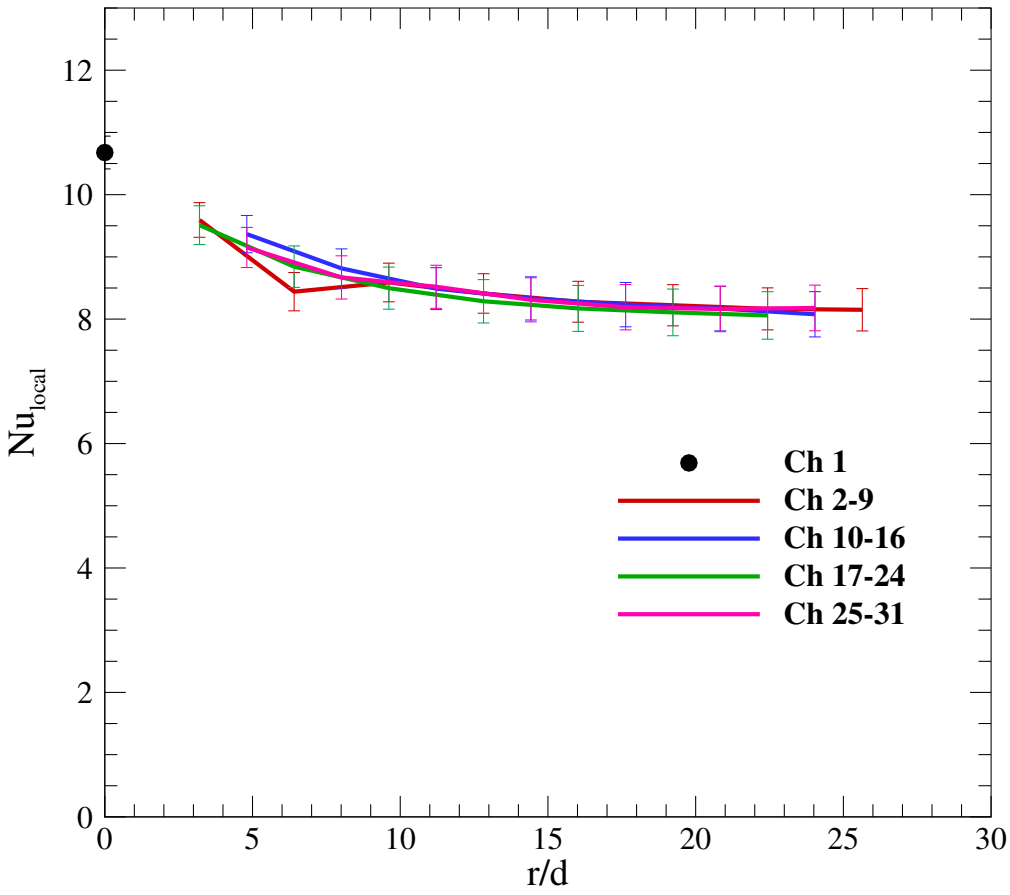

Figure 10: Local Nusselt number vs. r/d for case T_1 (Re= 12000, $r/d = 2.5$).

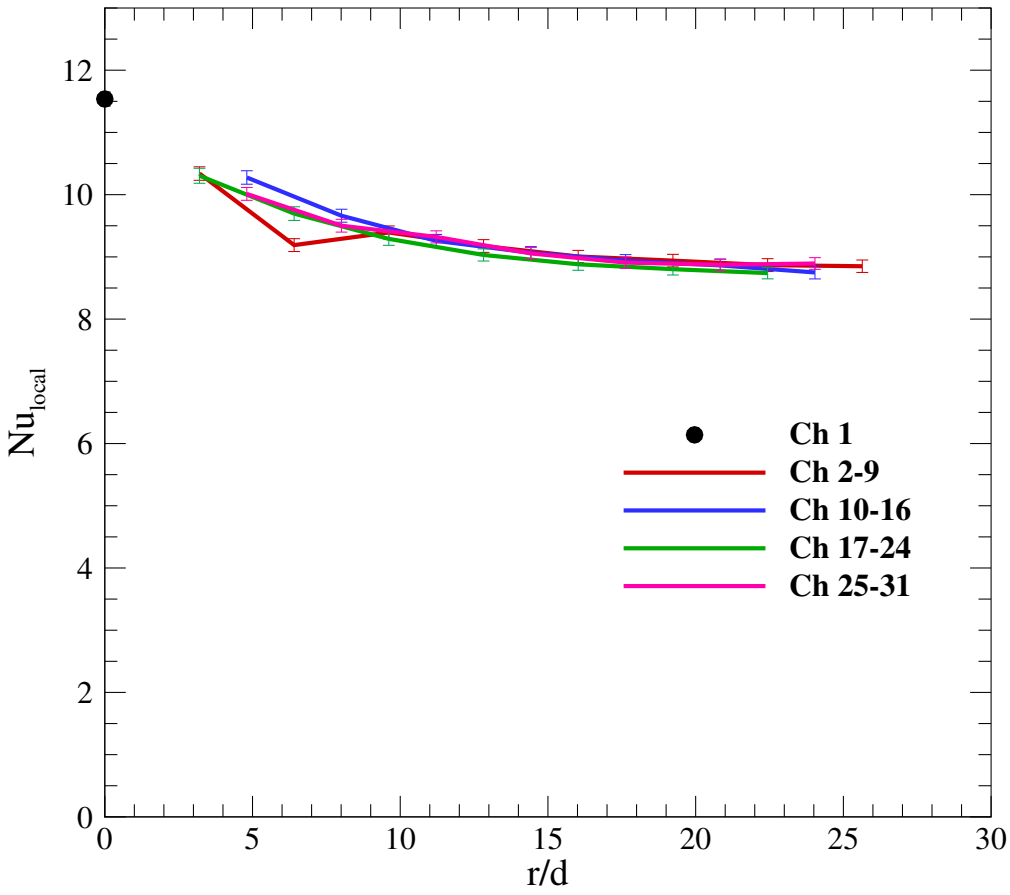

Figure 11: Local Nusselt number vs. r/d for case T_2 (Re= 12000, $r/d = 10$).

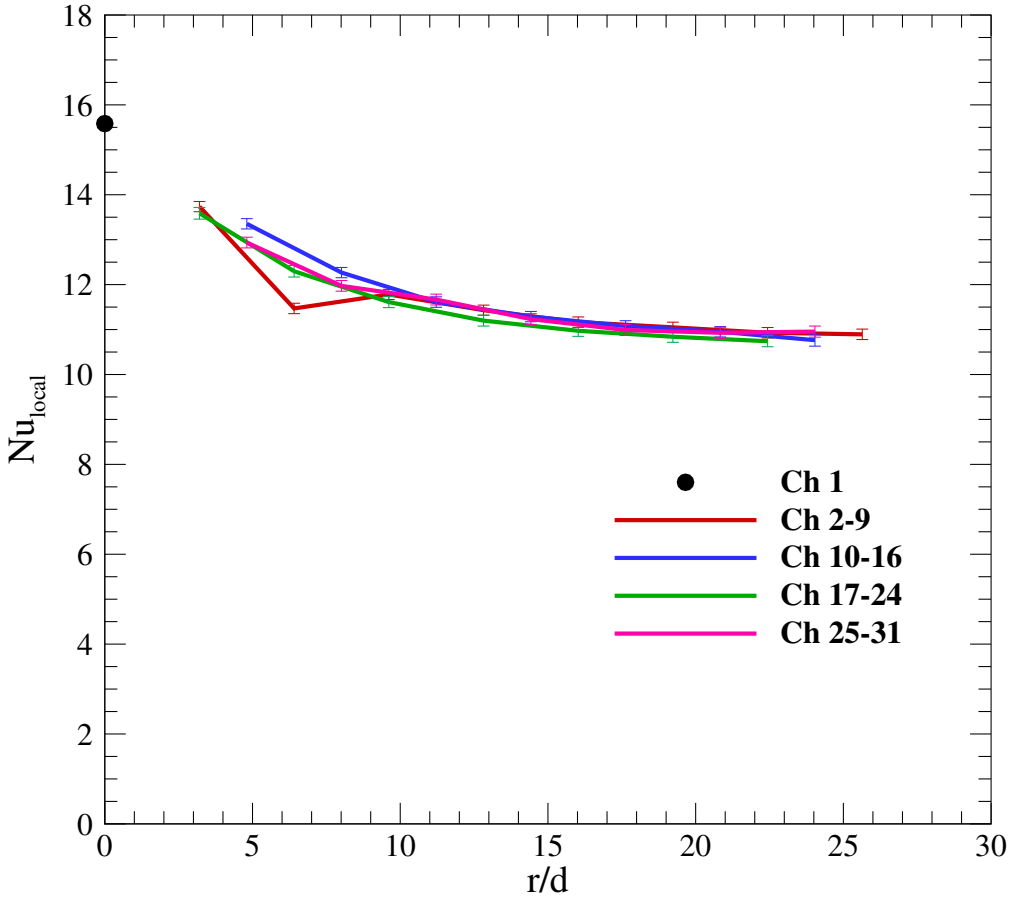

Figure 12: Local Nusselt number vs. r/d for case T_3 (Re= 20000, $r/d = 2.5$).

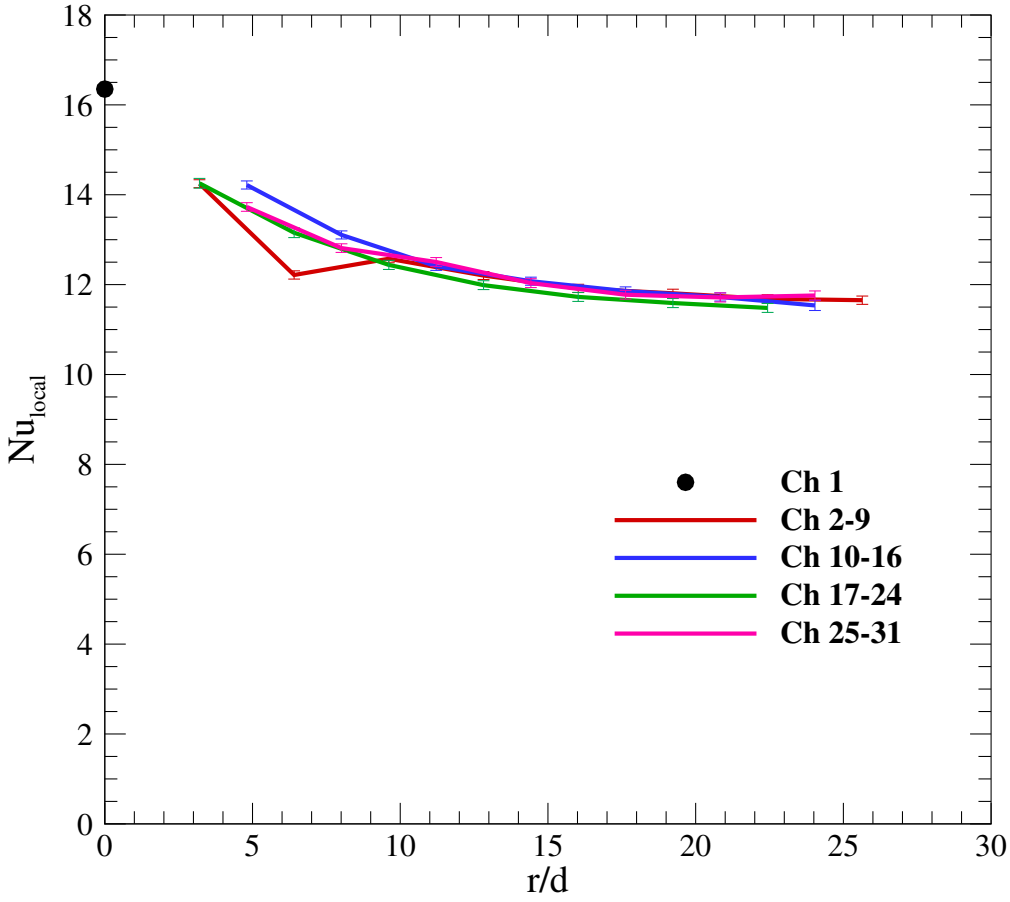

Figure 13: Local Nusselt number vs. r/d for case T_4 (Re= 20000, $r/d = 10$).

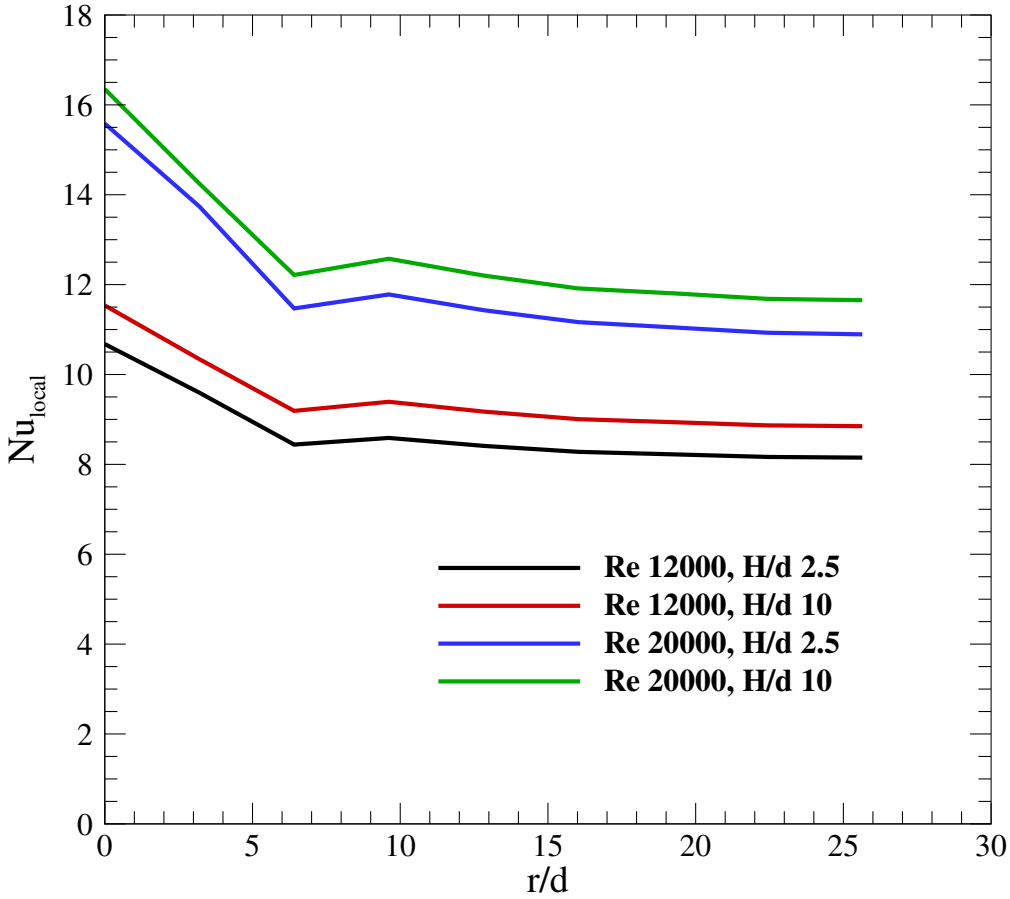

Figure 14: Local Nusselt for channels 1 through 9 at each r/d for all cases.

4.2 Normalized Local Nusselt Number

In this section the local Nusselt number normalized with the stagnation Nusselt is plotted vs. r/d, where r is the radial distance from the center, for each case. Figures 15, 16, 17, and 18 show the normalized local Nusselt number as a function of r/d for cases T_1, T_2, T_3, and T_4 (presented in table 2), respectively. These figures again predict the same behaviour as the previous section. However, this time, the normalized graph of Nusselt vs. r/d does not vary much with changing H/d. Figure 19 shows the value of the normalized Nusselt for channels 1 through 9 at each r/d for test cases T_1, T_2, T_3, and T_4. As seen in this figure the normalized Nusselt does not change very much with changes in H/d. However, there are considerable changes in normalized Nusselt with Reynolds number.

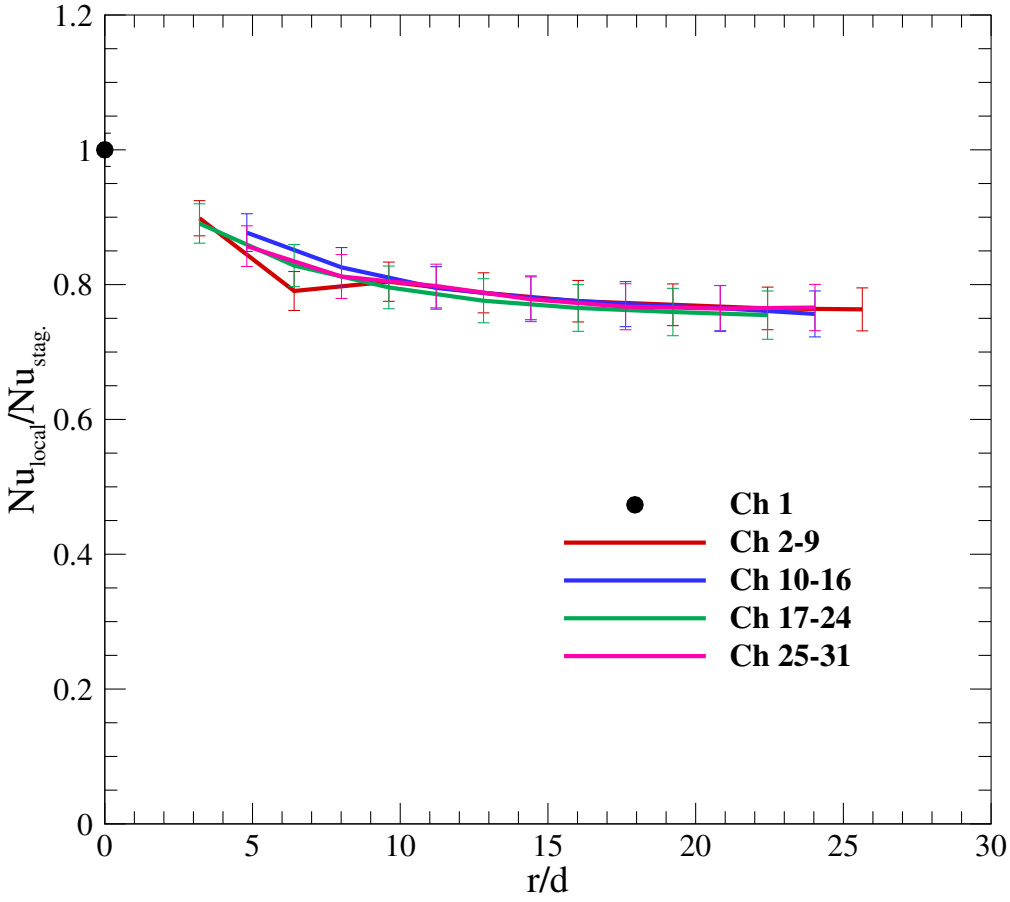

Figure 15: Normalized local Nusselt number vs. r/d for case T_1 (Re= 12000, $r/d = 2.5$).

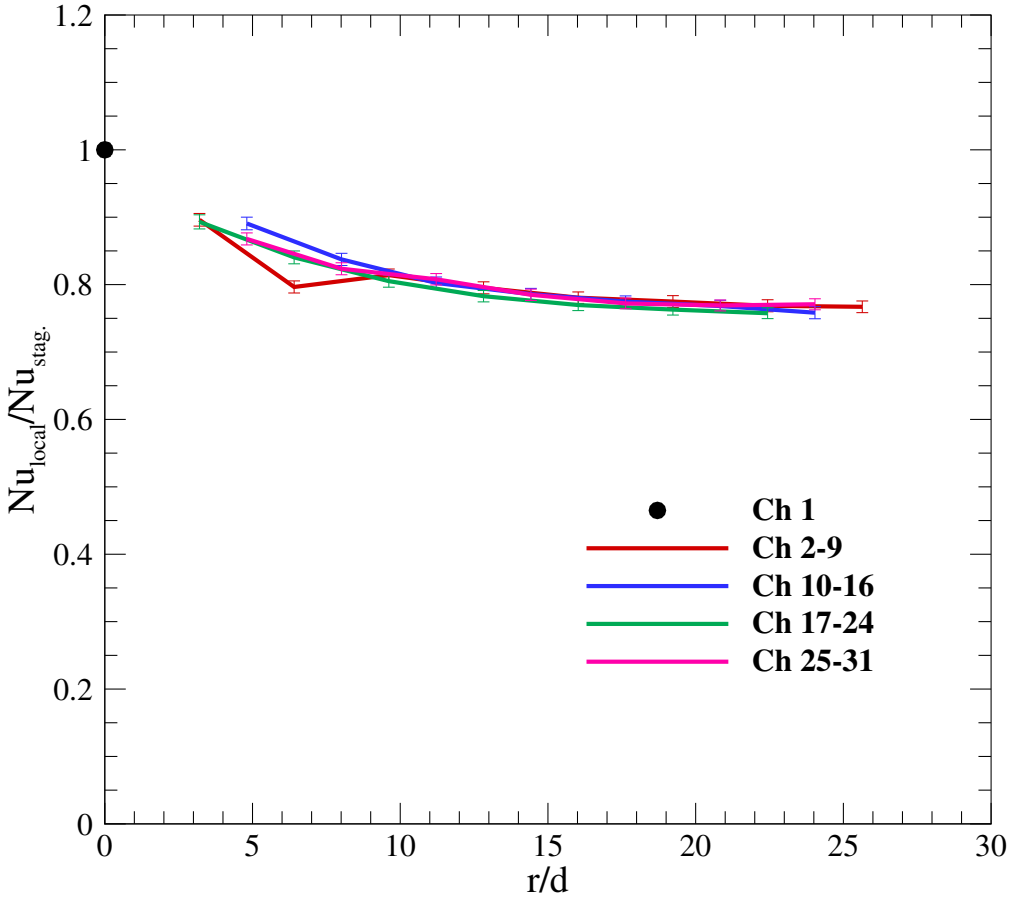

Figure 16: Normalized local Nusselt number vs. r/d for case T_2 (Re= 12000, $r/d = 10$).

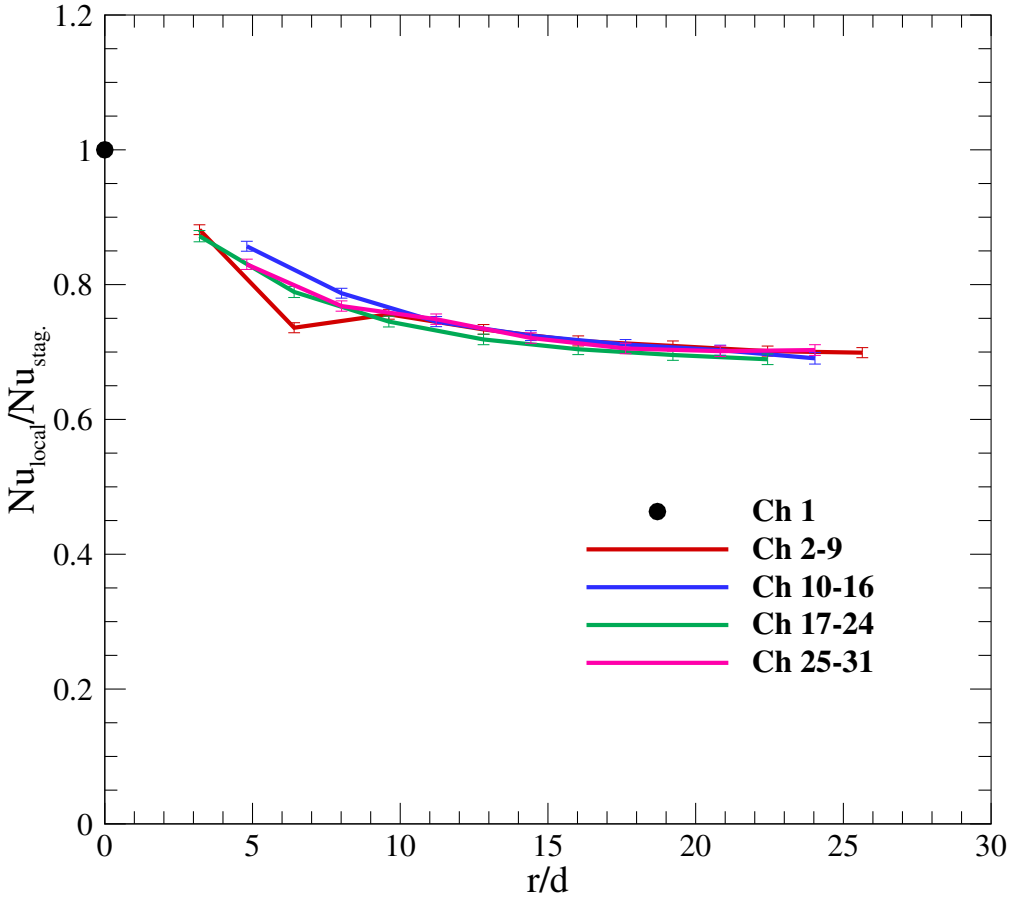

Figure 17: Normalized local Nusselt number vs. r/d for case T_3 (Re= 20000, $r/d = 2.5$).

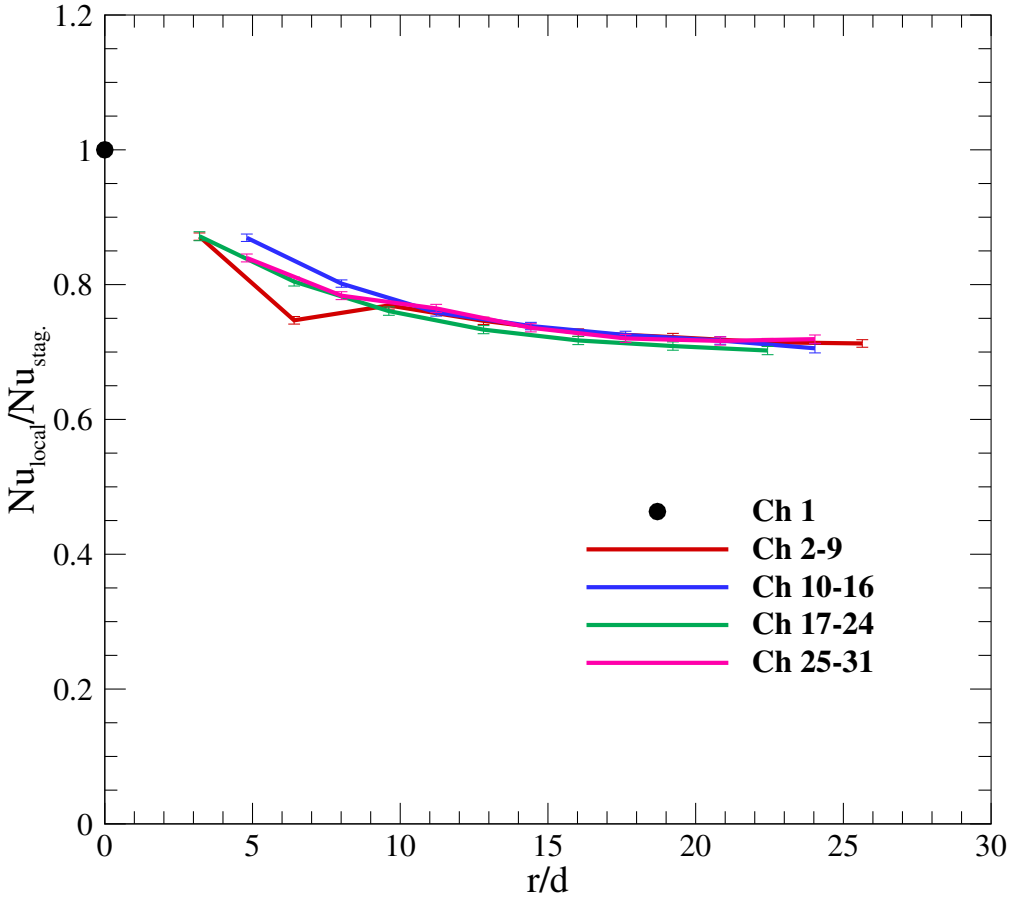

Figure 18: Normalized local Nusselt number vs. r/d for case T_4 (Re= 20000, $r/d = 10$).

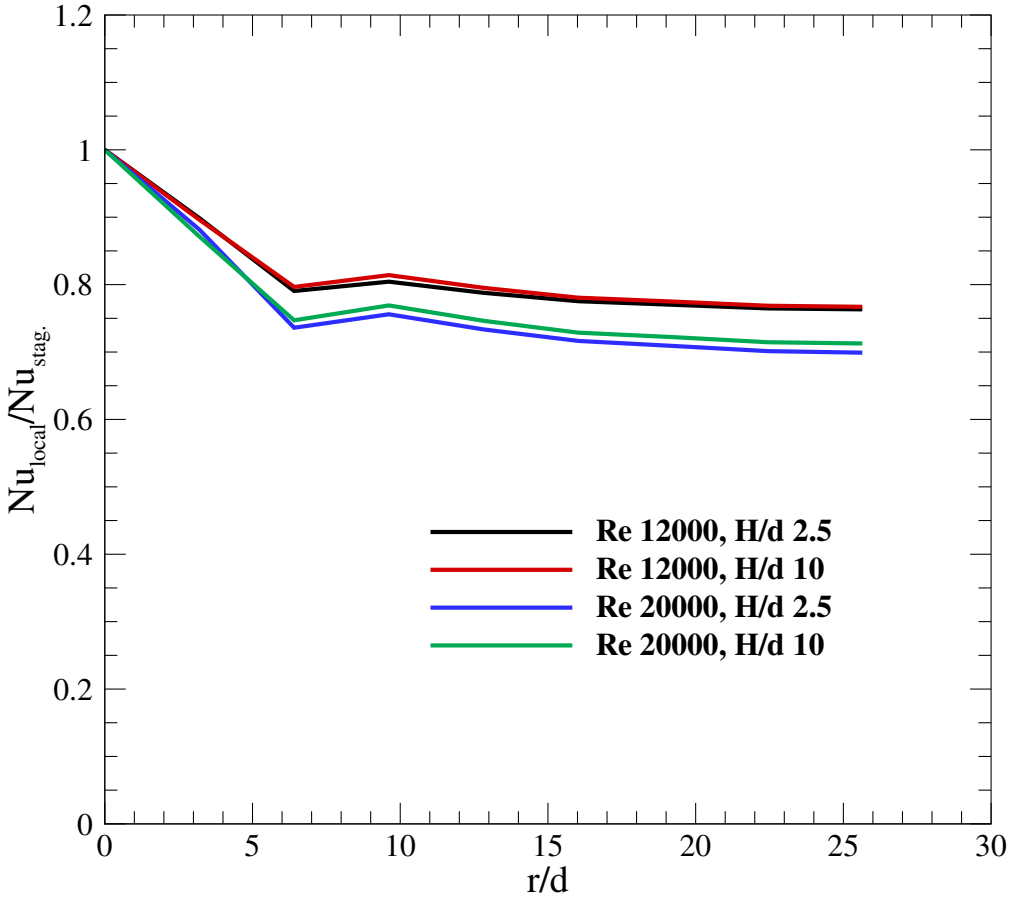

Figure 19: Normalized Nusselt for channels 1 through 9 at each r/d for all cases.

5 Average Nusselt Number

To calculate the average values of Nusselt number along the radius we will need a method of weight averaging. Because we have a discrete set of measurements, a numerical integration can be used. Trapezoidal method can be utilized in this context which gives good accuracy as well. The average Nusselt along the radius can be expressed as the following equation.

$$\mathrm{Nu}_{\mathrm{average}} = \frac{1}{L}\int_0^L \mathrm{Nu}dr \tag{10}$$

In which L is the length of each thermocouple tentacle. Using trapexoidal numerical integration method we get the following.

$$\mathrm{Nu}_{\mathrm{average}} = \frac{1}{L}\sum_{1}^{N}\left[(r_i - r_{i-1})\frac{\mathrm{Nu}_i + \mathrm{Nu}_{i-1}}{2}\right] \tag{11}$$

Now we can easily average these four numbers for each test case and get the average value. The results are presented in table 3. Also in this table the average values of Nusselt from the correlation presented by [2], are calculated. This equation is presented as follows. These set of equations works well for $2000 < \mathrm{Re} < 400000$ and $2 < H/d < 12$. Prandtl number for the working fluid (air) in our experiment is 0.7296. Keep in mind that in this case we have to calculate the average Nusselt from correlation for each tentacle and then average these values like we did with the numerical integration.

$$\frac{\overline{\mathrm{Nu}}}{\mathrm{Pr}^{0.42}} = G\left[2\mathrm{Re}^{0.5}(1 + 0.005\mathrm{Re}^{0.55})^{0.5}\right] \tag{12}$$

$$G = 2A_r^{0.5}\frac{1 - 2.2A_r^{0.5}}{1 + 0.2(\frac{H}{d} - 6)A_r^{0.5}} \tag{13}$$

$$A_r = \frac{d^2}{4r^2} \tag{14}$$

As we can see in this table, the average values from numerical integration and the correlation by [2] are very close. The correlation predicts that increasing H/d will cause the average Nu to decrease, which is contrary to what we have found. This might be because of the time duration of our experiment which was not really reaching a steady state. Also, other sources of error can affect this result. However, the results still are very close to the analytical correlation which is good.

Table 3: Average value of Nusselt for each test case.

Test	Average Nu	Nu correlation by [2]
T_1	8.70342	9.2243
T_2	9.47357	8.9782
T_3	11.9869	12.7787
T_4	12.7635	12.4377

6 Sources of Error

Conducting experimental studies on heat transfer will always include many sources of error. There are a few sources of error in this experiment as well. Most of these error cannot be avoided due to test conditions and facility. These errors are listed in the following.

- Variations in air properties near the hot surface of the plate.

- The tests were not fully at steady state when we finished our testing.
- Emissivity of the plate was not constant at different points and different times.
- Solar radiation from outside.
- The presence of four people near the testing device and moving around.

7 Uncertainty Analysis

The term uncertainty is used to refer to a "possible value that an error may have". It is necessary to make a distinction between single sample and multiple sample uncertainty analysis. The distinction hinges on whether or not a "large" or "small" number of independent data points are taken at each test point and on how the data are handled. Uncertainties for the experimentally measured lift coefficient are evaluated in this section. The methodology for estimating uncertainties follows the AIAA S-071 Standard as presented in [3] for multiple tests (sections 6.1 and 6.3). Uncertainties include various parameters such as; reading errors, measurement errors, calibration error and so on. Sources of error of the present experiment can be summarized as:

- Measurement system errors
- Noise or random errors
- Reading errors
- Calibration errors
- Errors in airfoil geometry and manufacturing which accounts for the errors in pressure tap positions as well

Consider a variable x_i which has a known uncertainty δx_i. The form of representation of this variable and its uncertainty is:

$$x_i = \overline{x}_i \pm \delta x_i \quad [P\%] \tag{15}$$

In this equation, $\overline{x}_i$ is the best estimate of x_i. Also, there is $P\%$ chance that this statement is true. Further, δx_i represents 2σ for a single sample analysis in which σ is the standard deviation of population of a possible data set.

The results R of the experiment is assumed to be calculated as a function of a number of independent parameters represented by:

$$R = R(x_1, x_2, \ldots, x_m) \tag{16}$$

The effect of the uncertainty in a single measurement on the calculated results is:

$$\delta R x_i = \frac{\partial R}{\partial x_i} \delta x_i \tag{17}$$

$\frac{\partial R}{\partial x_i}$ is the sensitivity coefficient for the results R with respect to measurement x_i. When several independent variables are used in the function of R, the individual terms are combined by RSS method.

$$\delta R = \left(\sum_{i=1}^{m} \left(\frac{\partial R}{\partial x_i} \delta x_i \right)^2 \right)^{0.5} \tag{18}$$

Unlike a multiple sample experiment, in which the variable error in a set of measurements can be determined from variance, simple sample experiments require an auxiliary experiment in order to estimate the variable component of the uncertainty. This usually takes the form of a set of independent observations of the process at a representative test condition over a representative interval of time. The principal difficulty here is finding σ, the standard deviation of the population from a smaller than infinite set of observations. σ is different from the standard deviation of the set of observations made in the auxiliary experiment, but can be estimated from it. In single sample uncertainty analysis, each measurement is assigned three uncertainty value; zero, first and Nth order uncertainties.

7.0.1 Zero order uncertainty

The zero order uncertainty of a measurement is the RSS combination of all the fixed and random uncertainty components introduced by the measuring system.

7.0.2 First order uncertainty

The first order uncertainty of a measurement describes the scatter that would be expected in a set of observation using the given apparatus and instrumentation system, while the observed process is running. The first order uncertainty includes all effects of process unsteadiness as well as the variable error effects from the measuring system. The first order uncertainty interval must be measured in an auxiliary experiment.

7.0.3 Nth order uncertainty

The Nth order uncertainty of a result is a measure of its overall uncertainty, accounting for all sources of fixed and variable errors. This is the value that should be reported as the overall uncertainty. The Nth order uncertainty is calculated as the RSS combination of the first order uncertainty and the fixed errors from every source.

8 Conclusion

In this lab experiment, we conducted tests to see the effect of Reynolds number as well as nozzle distance from the wall on the heat transfer from a flat plate. The air jet is located directly above the center point of the plate and is impinging on the plate at a right angle. The goal was to characterize the forced convection heat transfer with Nusselt number. The results show that increasing Reynolds number results in an increment in convection heat transfer.

Further, increasing the value of H/d also increases the heat transfer which is contrary to the analytical correlation. It seems that if the nozzle is closer to the flat plate, we should get more heat transfer and higher Nusselt numbers which is consistent with the analytical correlation. This differences in results might be because of the state of the experiment which did not reach steady state. Also, there were many more sources of error in our experiment which are discussed in previous sections.

References

[1] B. HAN and R. J. GOLDSTEIN, "Jet-impingement heat transfer in gas turbine systems," *Annals of the New York Academy of Sciences*, vol. 934, no. 1, pp. 147–161, 2001.

[2] T. Aicher and H. Martin, "New correlations for mixed turbulent natural and forced convection heat transfer in vertical tubes," *International Journal of Heat and Mass Transfer*, vol. 40, no. 15, pp. 3617–3626, 1997.

[3] F. Stern, M. Muste, M.-L. Beninati, and W. E. Eichinger, "Summary of experimental uncertainty assessment methodology with example," tech. rep., IIHR Report, 1999.

Appendix A

The complete set of data calculation are attached as spread sheet files.